

Interaction of Vegetation and Atmospheric Dynamical Mechanisms in the Mid-Holocene African Monsoon*

KATRINA HALES AND J. DAVID NEELIN

Department of Atmospheric and Oceanic Sciences, and Institute of Geophysics and Planetary Physics, University of California, Los Angeles, Los Angeles, California

NING ZENG

Department of Atmospheric and Oceanic Science, and Earth System Science Interdisciplinary Center, University of Maryland, College Park, College Park, Maryland

(Manuscript received 31 January 2005, in final form 2 December 2005)

ABSTRACT

Paleoevidence indicates that generally wetter conditions existed in the Sahara during the mid-Holocene. Climate modeling studies addressing this issue generally agree that mid-Holocene values of the earth's orbital parameters favored an enhanced North African summer monsoon but also suggest that land surface and vegetation feedbacks must have been important factors. Attempts to reproduce the "green" mid-Holocene Sahara in model studies with interactive vegetation may be interpreted to indicate that the problem is highly sensitive to the atmospheric dynamics of each model employed. In other work, dynamical mechanisms have been hypothesized to affect monsoon poleward extent, particularly ventilation, by import of low-moist static energy air to the continent. Here, interactive vegetation and the ventilation mechanism are studied in an intermediate complexity atmospheric model coupled to simple land and vegetation components. Interactive vegetation is found to be effective at enhancing the precipitation and vegetation amount in regions where the monsoon has advanced because of changes in orbital parameters or ventilation yet not very effective in moving the monsoon boundary if ventilation is strong. The poleward extent of the mid-Holocene monsoon and the steppe boundary are primarily controlled by the strength of ventilation in the atmospheric model. Within this boundary, the largest changes in monsoon precipitation and vegetation occur when interactive vegetation and reduced ventilation act simultaneously, as these greatly reinforce each other.

1. Introduction

a. The "green Sahara" problem

In the mid-Holocene [approximately 6000 yr before present (B.P.)], paleoevidence indicates that the Sahara region of Africa was substantially more vegetated than today. The extent of vegetation in the mid-Holocene was reconstructed by the BIOME 6000 project from paleodata (Prentice and Webb 1998; Prentice et al. 1998; Jolly et al. 1998b). The BIOME 6000 project compiled paleodata from ancient dune and lake sediments

(Sarnthein 1978; Street and Grove 1976; Street-Perrott and Harrison 1985; Yu and Harrison 1996), archaeological evidence (Petit-Maire 1989), and marine and terrestrial pollen and macrofossils (Dupont 1993; Street-Perrott and Perrott 1993; Jolly et al. 1998a,b). The reconstruction indicates that grassland and shrubland existed over much of the present-day Sahara. This mid-Holocene green Sahara problem implies substantial differences in rainfall pattern, presumably associated with changes in the summer monsoon circulation (Joussaume and Taylor 1995; Joussaume et al. 1999). Mid-Holocene orbital parameters imply greater Northern Hemisphere summer insolation at 6 kyr B.P., and therefore, more energy at the surface that is potentially available to drive the monsoon circulation. However, the mechanisms that translate differences in radiative forcing into changes in precipitation and vegetation appear to be complex.

The Paleoclimate Modeling Intercomparison Project

* Institute of Geophysics and Planetary Physics Publication Number 6213.

Corresponding author address: Dr. J. David Neelin, Department of Atmospheric Sciences, University of California, Los Angeles, 405 Hilgard Avenue, Los Angeles, CA 90095-1565.
E-mail: neelin@atmos.ucla.edu

(PMIP; Joussaume and Taylor 1995; Joussaume et al. 1999; Braconnot 2000) compared results from several general circulation models (GCMs) using 6 kyr B.P. orbital parameters. In the PMIP experiments, the atmospheric GCMs with 6 kyr B.P. orbital forcing do not extend precipitation north of 18°N, indicating that 6 kyr B.P. orbital changes alone can bring increased precipitation to the Sahel but not farther north into the Sahara Desert. Although these models have a range of prescribed albedo, using present-day albedo in the Sahara may contribute to the failure of the simulated mid-Holocene monsoon to advance farther into the Sahara in some cases. However, as investigated in Bonfils et al. (2001), even with a relatively low albedo value, the simulated monsoon change does not match the paleodata. This suggests including a prescribed green Sahara or using an interactive vegetation model. Many studies have pursued this approach; for instance, simulations with prescribed vegetation changes (Street-Perrott et al. 1990; Kutzbach et al. 1996a,b) or interactive vegetation (Claussen and Gayler 1997; Texier et al. 1997; Pollard et al. 1998; Doherty et al. 2000) enhance the monsoon to varying degrees. Atmospheric GCMs coupled with ocean models show positive feedback from the ocean (Hewitt and Mitchell 1998; Kutzbach and Liu 1997; Braconnot et al. 2000). Simulations including both interactive vegetation and ocean model components have come closer to reconstructions (Ganopolski et al. 1998a,b; Braconnot et al. 1999).

b. Dynamical mechanisms affecting monsoon extent

Recent developments in monsoon theory suggest that the poleward extent of all major monsoons is substantially affected by the dynamical processes (Chou and Neelin 2003; Chou et al. 2001) described below. It is hypothesized that these will be relevant to the mid-Holocene case. The ventilation mechanism is the import of low moist static energy air from the ocean (where heat storage opposes summer warming) to the continent. Thus the ventilation can limit the poleward extent of the monsoon by advecting cooler air that has less moisture than required to reach the convection threshold over a warm continent. The import to continents is by wind via advection terms in temperature and moisture equations. In numerical models, small-scale advection represented as diffusion is part of the ventilation, since it participates in moving low moist static energy air over the continent. This can be especially important where winds become small or at the edge of the convergence zone where moisture gradients can be large. The diffusion tends to spread the effect of an air mass imported by advection.

Chou and Neelin (2003) examined the ventilation ef-

fect in present-day monsoon systems. Compared to the other monsoon systems studied, the African monsoon had the least impact from a reduction in ventilation. They tested the hypothesis that present-day high albedo values over North Africa limit the impact from other mechanisms, namely, the ventilation effect. In experiments with lower albedo over North Africa, ventilation was found to have precipitation impacts similar in magnitude to those found in other monsoon systems. One anticipates from this that when albedo interacts through vegetation, there will be an interplay between the ventilation mechanism and albedo feedbacks.

Related experiments from Su and Neelin (2005) provide a starting point for the experiments described here. They examine the interplay of the ventilation mechanism with changes in albedo in the mid-Holocene African monsoon, without interactive vegetation but with a more detailed examination of atmospheric dynamics. With albedo specified from observed data, they find that 6 kyr B.P. orbital parameters produce increased monsoon intensity and extent to about 20°N. When the high albedo region in North Africa is reduced to 0.2, akin to prescribing a grass-type vegetation albedo over the whole Sahara, some monsoon impacts occur but strong ventilation can prevent the monsoon from advancing very far. Experiments affecting ventilation cause the monsoon to advance much farther poleward. We consider similar experiments, but ones including an interactive vegetation component.

De Noblet-Ducoudré et al. (2000) coupled the same biogeography model [BIOME version 1.0 of Prentice et al. (1992)] to two different GCMs. They were motivated by the results of Claussen and Gayler (1997) that showed realistic greening of the western Sahara, while Texier et al. (1997), using a different GCM, showed a lack of greening. They found pronounced differences between the models in surface pressure, large-scale convergence/divergence (in both present day and the mid-Holocene). Clearly, the atmosphere is making the difference in this case, and the hypothesis here is that this is due to differences in the dynamical mechanisms.

c. Synergy

The present study aims at understanding the relative importance and, especially, the synergy that is hypothesized to occur between vegetation feedbacks and dynamical mechanisms. Weakening the ventilation or letting the vegetation increase with precipitation are each known to affect the monsoon separately. When both effects occur simultaneously, they may well be more than additive. The albedo distribution depends on the precipitation via the vegetation, so for moderate ventilation, there is a positive feedback on any regions that

the monsoon reaches. How this affects the monsoon in terms of advancing the poleward margin of the monsoon versus enhancing precipitation behind the poleward margin is among the questions of interest.

Section 2 provides a brief summary of the atmospheric and land surface models. The vegetation model is presented and the simulation of North African present-day climate is assessed for uncoupled and coupled model versions in section 3. In section 4, the mid-Holocene simulation is presented, with a series of experiments aimed at quantifying insolation, vegetation feedback, and ventilation impacts.

2. Atmosphere–land surface model summary

a. Atmospheric model: QTCM

The quasi-equilibrium tropical circulation model (QTCM) of Neelin and Zeng, version 2.3 (Neelin and Zeng 2000; Zeng et al. 2000), is our tool to study the interaction of atmospheric dynamics, vegetation, and land processes. The QTCM is an atmospheric model of intermediate complexity designed to capture tropical climate behavior. Based on the primitive equations, the QTCM's main simplification (from GCM-type formulation) is the use of tailored basis functions for temperature and winds that allow severe truncation in the vertical because of assumptions about convective closure. The formulation and analysis of simulations using the QTCM are discussed in Neelin and Zeng (2000) and Zeng et al. (2000). We run the model on a spatial grid from 78.75°N to 78.75°S at a resolution of 3.75° latitude \times 5.625° longitude.

b. Land surface model: SLand

The simple land surface model (SLand; Zeng et al. 2000) is simple compared to developed biophysical land surface parameterizations (Dickinson et al. 1993; Sellers et al. 1996a). While slightly more complex than the bucket model, since it imitates aspects of the biophysical models, it is much simpler than, for example, the land surface model developed by Xue (1991). The findings of the Project for Intercomparison of Land surface Parameterization Schemes (PILPS; Henderson-Sellers et al. 1993) suggest that a relatively simple model approximately captures the primary effects for climate simulation at time scales longer than diurnal and synoptic scales (Koster and Milly 1997). A thin land surface layer is used for the energy budget and a much thicker layer represents the root-zone water budget. The thermodynamic budget essentially yields zero net surface flux on time scales much longer than a day since the land heat capacity is small. Sensible heat fluxes are

calculated using the standard bulk formula, and evaporation has a formulation akin to the biophysical models, with a surface resistance similar to a stomatal resistance combined with the effects of root resistance in dry soil conditions (Dickinson et al. 1993). This resistance has a simple dependence on soil moisture; that is, resistance increases as the soil moisture decreases. In a single soil layer representing the root zone, interactive soil moisture (W) is driven by precipitation (P) minus evaporation and runoff:

$$\frac{\partial W}{\partial t} = P - E_I - E_B - E_T - R_s - R_g, \quad (1)$$

with parameterizations of interception loss (E_I), bare soil evaporation (E_B), and evapotranspiration (E_T). The spatial and temporal variability of rainfall and surface properties affect surface runoff (R_s ; the fast component) and subsurface runoff (R_g ; the slow component), parameterized similarly to more sophisticated land surface schemes (Shuttleworth 1988; Entekhabi and Eagleson 1989) but with simpler statistical assumptions (Zeng and Neelin 1999; Zeng et al. 2000). Bare soil evaporation is calculated from relative soil wetness and soil resistance. Evapotranspiration is calculated by

$$E_T = (r_s + r_a)^{-1} \rho_a [q_{\text{sat}}(T_s) - q_a], \quad (2)$$

where T_s is the surface temperature, ρ_a is air density, q_a is air humidity, q_{sat} is air humidity at saturation, r_a is the aerodynamic resistance (which depends on roughness height and surface winds), and r_s is the surface resistance with

$$r_s = g_s^{-1}, \quad (3)$$

where g_s (surface conductance) is parameterized on soil moisture, vegetation type, and leaf area index (LAI) as discussed in section 3a(2).

The land model includes five land surface types (Hales et al. 2004) based on observed vegetation class (DeFries and Townshend 1994). They are used to prescribe roughness length. When running with the vegetation model turned off, LAI is prescribed by a monthly climatology based on an observed 9-yr record from 1982 to 1990 (Los et al. 2000; Sellers et al. 1994).

3. Vegetation model: SVege

a. Formulation

In the interactive simple vegetation (SVege) model, we include two leaf area index variables representing total LAI (Λ) and a potential LAI (Λ_p). The potential LAI represents the maximum vegetation that the woody component can support. It essentially mimics the stem structure with a longer growth time, thus avoiding explicit modeling of woody biomass. The two

leaf areas therefore have different time scales—a shorter time scale to grow leaves and a longer one for wood. LAI is mainly given by soil moisture, which has a lag from precipitation with growth and loss terms. The equation for potential LAI (Λ_P) has the form

$$\frac{d\Lambda_P}{dt} = \left[\frac{\beta(w)(1 - e^{-k\Lambda})}{(1 - e^{-k\Lambda_{\max}})} \Lambda_{\max} - \Lambda_P \right] / \tau_m, \quad (4)$$

where $\beta(w)$ is the soil moisture dependence [$\beta(w) = \sqrt[6]{w}$], with w being relative wetness (ratio of soil moisture to field capacity), k is the extinction coefficient for photosynthetically active radiation (PAR; taken to be 0.75), Λ_{\max} is maximum LAI set to 6, and τ_m is the wood time scale, set to 20 yr for the experiments in this study.

For total LAI, Λ , we use

$$\frac{d\Lambda}{dt} = \left[\frac{\beta(w)(1 - e^{-k\Lambda})}{(1 - e^{-k\Lambda_M})} \Lambda_P - \Lambda \right] / \tau_v, \quad (5)$$

where τ_v is the leaf time scale, set to 2 weeks.

The growth term includes a saturation that can be interpreted to include light limitations with increasing vegetation; however, the leaf areas are not explicitly dependent on biotemperature, nutrient, and light factors. Since our focus is in the Tropics, we have made significant simplifications that would not apply to mid-latitude applications. Another caveat is that we use the same time scale for growth and loss terms. This neglects fire, deforestation, and other processes that would give a different decay time. A minimum LAI of 0.1 is maintained in Eq. (5) as a simple way to initiate regrowth in the spring. Since it appears in the growth term only, it does not create any imbalance in carbon-biomass conservation. The details of the vegetation formulation could have some impact on detailed model results. For instance, tree growth requirements would limit the maximum vegetation growth rate. However, in the problems considered here, external conditions are not changing on decadal time scales. The decadal time scale (τ_m) is important because it is substantially longer than the annual time scale, but the results here are not sensitive to exactly how much longer. The leaf time scale (τ_v) is important in representing the monsoonal variations prominent in the region.

Land surface albedo and surface conductance are calculated from LAI using parameterizations developed in Hales et al. (2004); see sections 3a(1) and 3a(2) below.

1) SURFACE ALBEDO

In our simplified experimental design, we only consider leaf area index dependence in our surface albedo parameterization for most regions. Generally, surface

albedo decreases with increasing vegetation amount because of the high absorption of PAR by plants. We use this relationship to parameterize surface albedo; other land surface schemes include more complex behavior (see, e.g., Wright et al. 1996). An analysis of observed datasets of LAI [the second International Satellite Land Surface Climatology Project (ISLSCP II) total LAI; Los et al. 2000; Sellers et al. 1994, 1996b)] and albedo [Earth Radiation Budget Experiment (ERBE) snow-free surface albedo; Barkstrom et al. 1990] leads us to use the following form (Hales et al. 2004):

$$A_s = a - b(1 - e^{-ck\Lambda}), \quad (6)$$

where A_s is land surface albedo, $a = 0.3352$, $b = 0.1827$, and $c = 1.733$ are constants determined by the fit of the curve, and k is as in Eq. (4).

For bare ground (specified to be regions with LAI less than 0.48), albedo is assigned by a simple linear relation with a maximum of 0.42 in the absence of vegetation. Since the minimum value of LAI allowed in SVEge is 0.1, the maximum surface albedo is 0.38. Over much of the Sahara, this minimum vegetation condition is met under present-day conditions.

2) SURFACE CONDUCTANCE

The movement of moisture from the surface to the atmosphere is resisted by plant roots and stomates along with the soil surface. The parameterization of surface conductance, formulated in Zeng et al. (2000) and discussed further in Hales et al. (2004), uses a leaf-to-canopy scaling similar to Sellers et al. (1996a,b), Zeng and Neelin (2000), and Zeng et al. (1999). Surface conductance, g_s , is parameterized as

$$g_s = g_{s_{\max}} \beta(w)(1 - e^{-k\Lambda})/k, \quad (7)$$

where $\beta(w)$ is the soil moisture dependence as in the LAI equation, and $g_{s_{\max}}$ is 6.67 mm s^{-1} for the tropical rain forest and 5 mm s^{-1} for all other vegetation classes. Similar to other land surface schemes [e.g., the Biosphere–Atmosphere Transfer Scheme (BATS); Dickinson et al. 1993], the conductance includes a dependence on vegetation class in the minimum resistance to address differences in vegetation structure.

b. Model validation

Figures 1 and 2 show tests of the land surface and vegetation model alone and with the fully coupled system (averages are shown for the last 50 yr of the 150-yr runs in these and subsequent model figures). The LAI produced with forcing by observed precipitation (Xie and Arkin 1997) and with the coupled model for August–October is compared to observed LAI (ISLSCP)

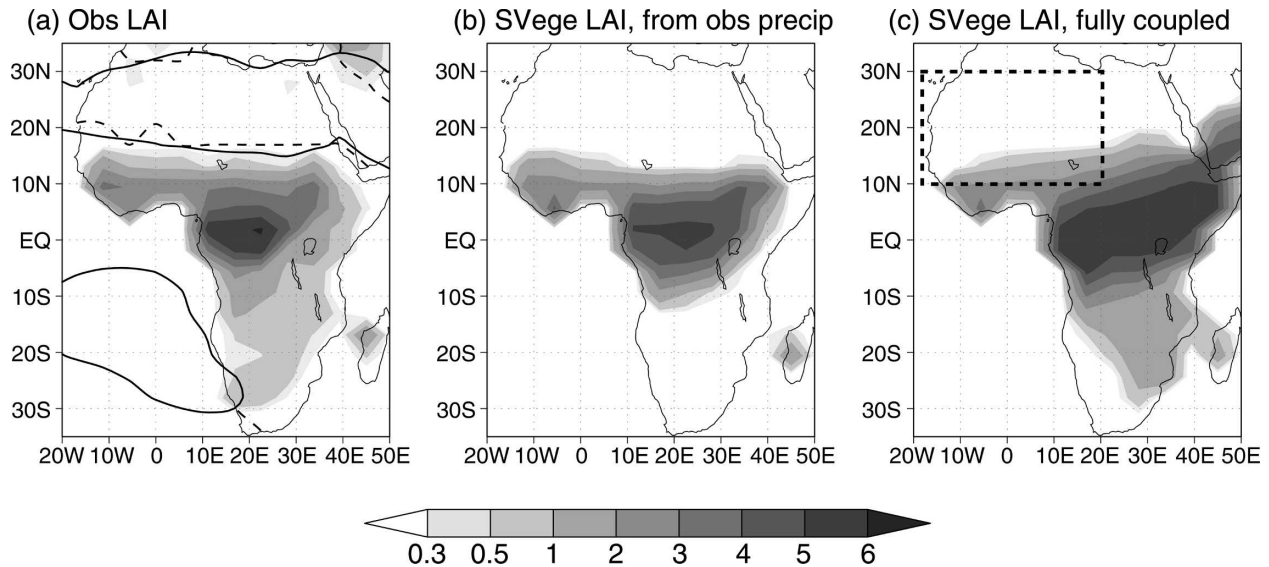


FIG. 1. August–October (ASO) LAI for (a) observed ISLSCP LAI, (b) SVEge–LAI forced by observed precipitation, and (c) SVEge–LAI in a fully interactive run. The present-day 200 mm yr⁻¹ annual precipitation contour (solid line; Xie and Arkin 1997) and boundary of present-day barren desert (dashed line; DeFries and Townshend 1994) are added to (a) for reference.

in Fig. 1. The case forced by observed precipitation provides a full test of the soil moisture scheme combined with the vegetation scheme. In this case, SVEge produces LAI (Fig. 1b) largely consistent with observed LAI (Fig. 1a). The northward extent and gradient from rain forest to desert is well reproduced; however, higher LAI regions in central Africa have a broader eastward range than in observations.

For later reference, Fig. 1a includes the contour of present-day, 200 mm yr⁻¹ precipitation and the border of the present-day Sahara Desert estimated as the boundary of barren desert from DeFries and Townshend (1994; smoothed by averaging to the grid of the model used in this study). For present-day Africa, the 200 mm yr⁻¹ precipitation contour has reasonable correspondence with the boundary of barren desert. Based on this correspondence, 200 mm yr⁻¹ is sometimes used as a rule of thumb as the boundary for transition from desert to dry grassland [see variants in Joussaume et al. (1999) and Irizarry-Ortiz et al. (2003)]. The precipitation required to transition from barren desert to dry grassland is estimated to be an increase of 200 and 300 mm yr⁻¹ in the Sahara Desert region (Joussaume et al. 1999). Observed station rainfall in the interior of the Sahara, especially in the 24°–28°N range, is commonly less than 20 mm yr⁻¹, so the differences in using a 200 mm yr⁻¹ increase or 200 mm yr⁻¹ total rainfall are generally small.

Control Precip (mm/y): Interactive Vegetation

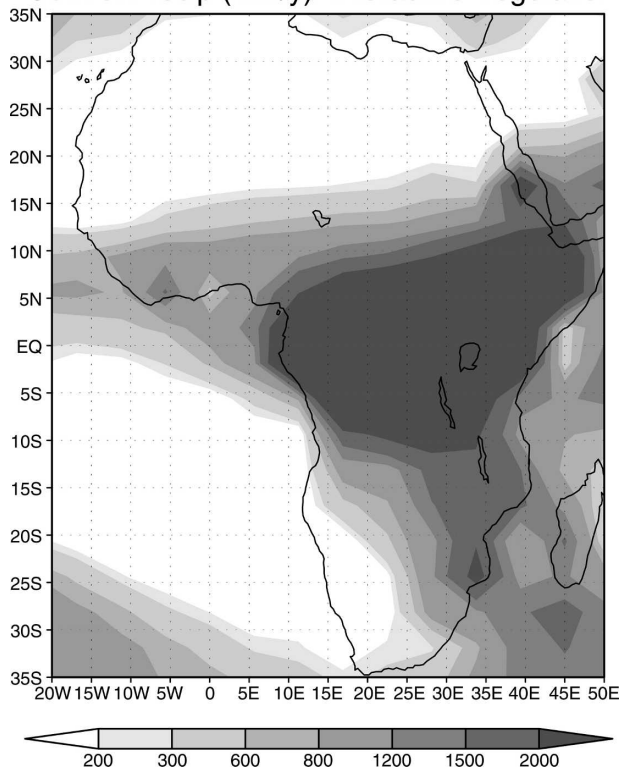


FIG. 2. Annual average simulated precipitation (mm yr⁻¹) from the coupled QTCM-SVEge run with present-day orbital conditions.

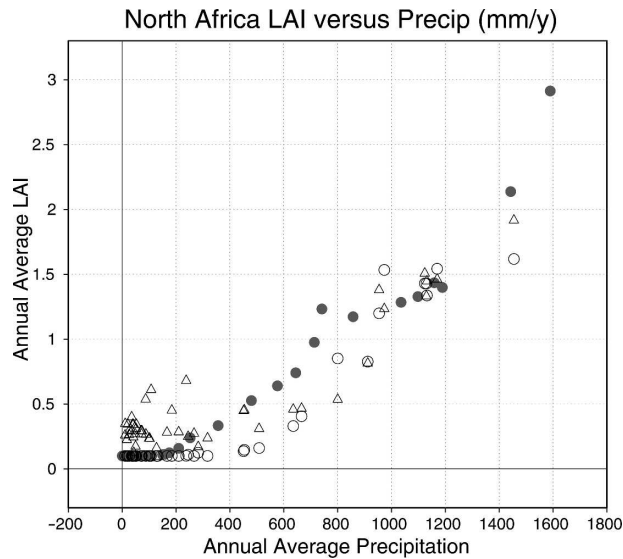


FIG. 3. Plot of annual average precipitation (mm yr^{-1}) versus annual average LAI for North Africa (10° – 30° N and 20° W– 20° E, land points only) with observed LAI (ISLSCP II, total LAI; Los et al. 2000; Sellers et al. 1994, 1996b) and observed precipitation (Xie and Arkin 1997; open triangles), SVEge–LAI forced by observed precipitation (open circles), and SVEge–LAI and precipitation from coupled runs (gray circles).

Annual average precipitation for the fully coupled SVEge–QTCM is shown in Fig. 2. Here the precipitation is higher than observed when east of approximately 25° E and the precipitation pattern between 0° and 20° N is less zonal than seen in observations (not shown). Since this model version is fully coupled, any error in precipitation or in soil moisture feeds back onto vegetation and precipitation. This climate drift seen in the precipitation pattern affects the coupled SVEge–LAI (Fig. 1c), producing an overly extensive rain forest region to the east of the observed high LAI zone, although not of as high LAI as observed in the maximum of the central African rain forest. The coupled model also roughly reproduces the zonal pattern of the vegetation gradient between 5° and 15° N, although it produces higher LAI in this latitude band in eastern Africa compared with observations. However, our region of focus is the Sahara and the gradient region of North Africa (highlighted by the box outline in Fig. 1c); in this region, the model performs reasonably well, and thus we consider the model a useful tool for the questions we consider here.

For North Africa land points (10° – 30° N and 20° W– 20° E), we compare the annual average precipitation–LAI relationship for model and observations in Fig. 3. The region included in this figure represents some moderate through low vegetation and desert regions relevant for the study here. SVEge–LAI closely follows

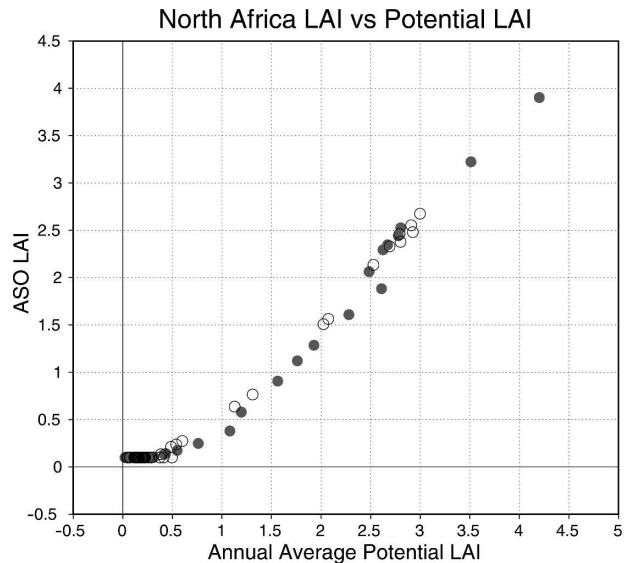


FIG. 4. Annual average potential LAI versus ASO LAI for North Africa (10° – 30° N and 20° W– 20° E, land points only) from runs forced by observed precipitation (open circles) and from fully coupled runs (gray circles).

the observed LAI when forced by observed precipitation, with somewhat lower values of SVEge–LAI for lower values of precipitation. When SVEge is running fully interactively, the model performs well in moderate and lower precipitation regions. For values of precipitation over 2500 mm yr^{-1} , the vegetation model LAI tends to saturate, so little error is incurred in LAI even if precipitation is high. In low precipitation regions, observed precipitation between 200 and 300 mm yr^{-1} does not strictly correspond to steppe/grassland conditions, and thus, we consider this threshold as only a guideline to indicate the transition from desert to steppe. For very low values of precipitation and LAI, the observed field has more scatter where the model does not, and thus, the model is conservative in producing vegetation in very low precipitation regions.

Annual average LAI is shown in Fig. 3, since it is not just instantaneous precipitation that matters but the vegetation type (including woody structure) that can be maintained over the seasonal cycle. Because potential LAI represents woody structure and is equilibrated on multiyear time scales, it tends to have a relationship to precipitation averaged over the whole year, although with some scatter since it is related to precipitation through soil moisture. Potential LAI is a significant factor in limiting rainy season LAI, as seen in Fig. 4. Especially in low vegetation regions, LAI cannot reach potential LAI and certainly cannot get larger even if precipitation is briefly large.

A sample of the modeled seasonal cycle is shown in

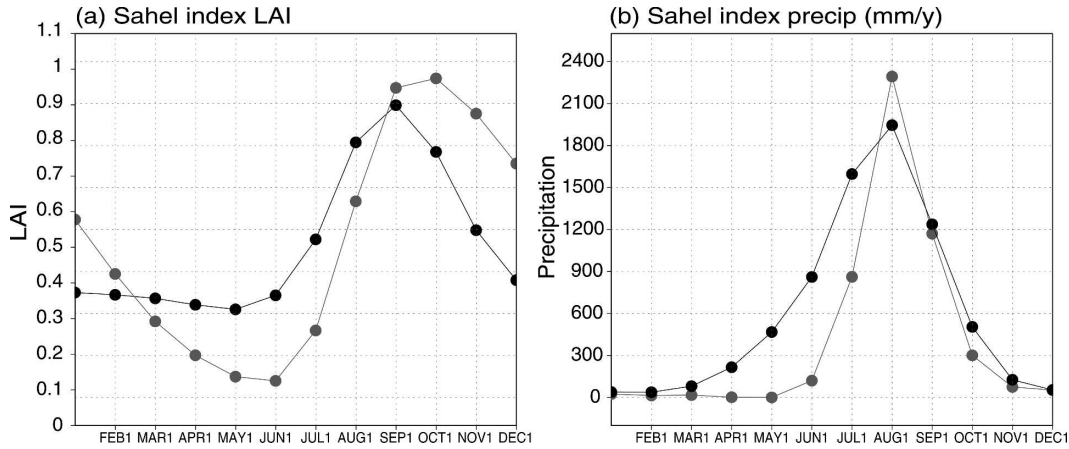


FIG. 5. The seasonal cycle in the Sahel (10° – 18° N and 20° W– 20° E) for (a) LAI and (b) precipitation (mm yr^{-1}) with observed values in black and coupled QTCM–SVege values in gray.

Fig. 5. We look at an index inside our region of interest, roughly the Sahel region, from 20° W to 20° E and from 10° to 18° N. SVege–LAI dips too low for the minimum and has about a 1-month lag from the observed. This seasonal lag is likely due to soil moisture lags relative to precipitation, since the model has its precipitation maximum in the same month as the observed but the model precipitation is too low leading up to the maximum.

4. Experiment results and discussion

a. Experimental design

Experiments were designed to understand some aspects of the mechanisms important to the extent of the mid-Holocene North African Monsoon. Table 1 provides a summary of the main experiments discussed in this paper.

First, we use either present-day (0 kyr B.P.) or mid-Holocene (6 kyr B.P.) orbital parameters in the radiation package. At 6 kyr B.P., perihelion was close to autumnal equinox, the tilt of earth's axis was about 0.7° greater than today, and the eccentricity of earth's orbit was slightly larger at 0.0187 (today it is 0.0167).

Second, we run with fully interactive vegetation or

with albedo fixed to the climatology produced by the present-day, interactive vegetation run. This shows a measure of the impacts of interactive vegetation. In the fixed-albedo runs, the standard QTCM evapotranspiration computation with present-day vegetation types is used. Note that we focus on the role of albedo because, as shown by Levis et al. (2004), it has the leading role.

Third, in order to examine the ventilation effect, the moisture advection and diffusion *anomalies* at each time step are reduced by one-third over the African continent (Su and Neelin 2005). Other studies targeting the ventilation have suppressed the advection terms $\mathbf{v} \cdot \nabla T$ and $\mathbf{v} \cdot \nabla q$ (Chou et al. 2001), or only reduced part of the advection associated with the nondivergent wind (Chou and Neelin 2003). For the case described here, the value of $[\overline{\mathbf{v} \cdot \nabla q} + \kappa \overline{\nabla^2 q} - (\overline{\mathbf{v} \cdot \nabla q} + \kappa \overline{\nabla^2 q})]$, where the overbar indicates the climatological mean from the control, is multiplied by a reduction factor r . This is designed to affect the control climatology as little as possible, although when we check this, there is some impact from transients. Note that if there is no change in moisture or winds, this experiment produces no effect. Thus, its aim is to reduce the effect of κ and \mathbf{v} on gradients of anomalous q induced by orbital parameter changes and vegetation feedbacks. We stan-

TABLE 1. Table of main experiments: combinations of present-day and mid-Holocene, fixed-albedo and interactive vegetation, and standard ventilation and reduced anomalous ventilation runs.

	Interactive vegetation	Fixed 0-yr SVege albedo
Standard ventilation	0 kyr B.P. control 6 kyr B.P. experiment	0 kyr B.P. control 6 kyr B.P. experiment
Reduced anomalous ventilation	6 kyr B.P. experiment	6 kyr B.P. experiment
Reduced diffusion	0 kyr B.P. control 6 kyr B.P. experiment	

dardly use a ventilation reduction factor of $r = 0.3$ as a means of producing—for sensitivity testing purposes—a strong reduction in the effect of ventilation on anomalies produced by the orbital forcing. The effect of using different values of this reduction factor was tested in Su and Neelin (2005). We use the reduction factor rather than the more drastic approach of setting this term to zero because while still very idealized, the reduction factor allows us to see the impact in a slightly more realistic, or at least more calibrated, circumstance. For instance, it is plausible that a model might overestimate the effect of ventilation in a particular region by a factor of 2 or 3, or that remote changes not represented in the model might produce a wind change that would partially cancel the climatological ventilation. The approach here gives a qualitative sense of how much impact that could produce.

We also examine two other sets of reduced ventilation experiments: a “total” ventilation case, where moisture advection and moisture diffusion are reduced by half at each time step over the African continent, and a simple reduced diffusion experiment, in which only moisture diffusion is reduced by a factor of 10, thereby reducing contribution to the ventilation. In these dynamical experiments, we do not try to control the climatology by artificial means, and thus, both experiments require a different control run than previously discussed. Both experiments are akin to what would occur when switching between two GCMs that have different climatologies and parameters. With this smaller ventilation, the convergence zone tends to extend poleward more easily.

We run each experiment for a continuous 150 yr. Runs reach an equilibrium after approximately 100 yr with an e -folding time of roughly 45 yr, although some adjustments still occur after 100 yr. In all figures, we show averages from the last 50 yr of the run. The sensitivity to initial conditions in North Africa was tested by initializing potential LAI over the Sahara to either 0.7 or 6 for “dry” and “wet” conditions, respectively. The wet and dry initial condition runs are essentially indistinguishable after approximately 100 yr. Additionally, when runs are started from the same potential LAI but with different soil moisture, atmospheric conditions, or other surface conditions, very little difference is noted.

For simplicity, the present-day sea surface temperature (SST) climatology is used similarly to the PMIP experiments. Also as in the PMIP experiments, approximate preindustrial and present-day CO_2 levels are used in the 6 kyr B.P. and 0 kyr B.P. runs, respectively. We do not address the role of oceanic feedback in this paper, but its effect is assessed using a mixed layer

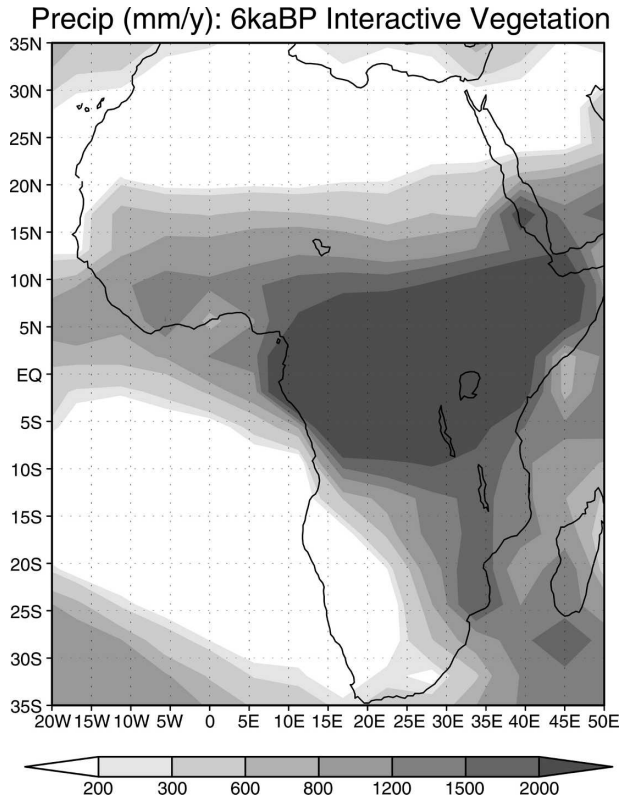


FIG. 6. Annual average precipitation (mm yr^{-1}) from the interactive vegetation run with mid-Holocene orbital conditions.

ocean model in Su and Neelin (2005). Ruddiman and Mix (1993) describe 6 kyr B.P. SST as not very different than today, although DeMenocal et al. (2000) note evidence for cooler coastal SSTs and more upwelling.

b. Mid-Holocene case

Implementing 6 kyr B.P. orbital conditions in the coupled model shows the effects of orbital changes plus interactive vegetation on the African monsoon. Annual average precipitation for present-day and mid-Holocene conditions is shown in Figs. 2 and 6, respectively, both with interactive vegetation. Precipitation moves north—the 200 mm yr^{-1} contour line advances from approximately 15° to 18°N in a roughly zonal pattern in western North Africa. Figure 7 shows the annual average precipitation change for mid-Holocene minus current conditions. The increase is zonal, but with larger anomalies to the west. Comparing the results to PMIP experiments, these experiments show further increased intensity and poleward extent. Using the 200 mm yr^{-1} line as a measure, the grassland boundary reaches approximately 20°N , whereas the BIOME 6000 vegetation reconstruction has several data points indicating grassland/steppe and a few xerophytic woods/scrubland points north of this latitude.

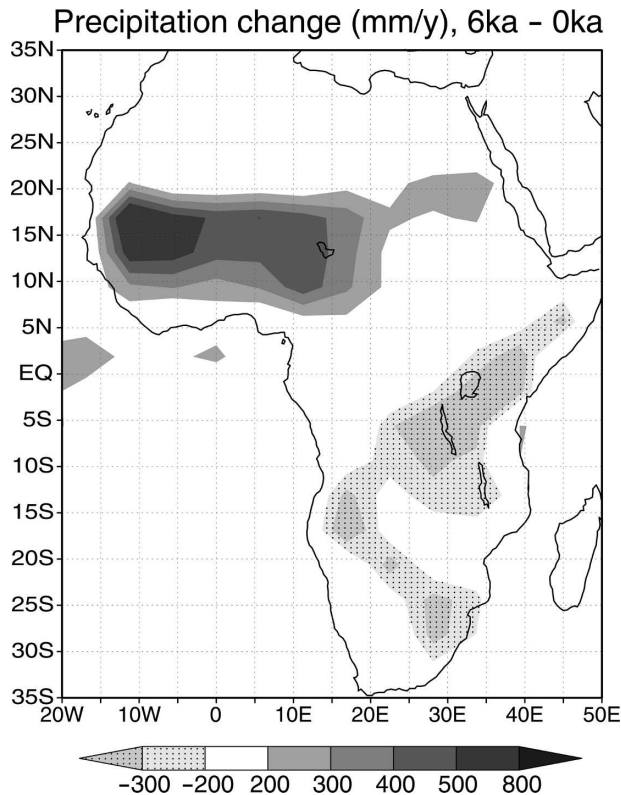


FIG. 7. Annual average precipitation change (mm yr^{-1}) from interactive vegetation runs with 6–0 kyr B.P. orbital parameters.

In comparison to more similar modeling efforts, Fig. 8 shows the June–August (JJA) mid-Holocene precipitation change from de Noblet-Ducoudré et al. (2000) using different GCMs coupled to the same vegetation model with initial green Sahara and present-day Sahara conditions. Although multiple equilibrium states have been found for the mid-Holocene Sahara by some (e.g., Irizarry-Ortiz et al. 2003), the difference between the de Noblet-Ducoudré et al. (2000) runs with the same vegetation model is a measure of the lack of convergence. The experiments described in de Noblet-Ducoudré et al. (2000) have asynchronous coupling, and with runs less than 20 yr long, the authors are not claiming to find multiple equilibria. Here we have added results from our coupled model 150-yr run for comparison. Generally, our anomaly is roughly in the range of their green Sahara anomalies, noting that the precipitation does drop off sooner to the north but extends farther north than when they start at present-day conditions. Runs from wet and dry initial conditions converge to the same solution after approximately 100 yr. Thus we find no multiple equilibria, as discussed in section 4a. If one uses a mean of their curves as a rough estimate of their unknown equilibrium, the QTCM sen-

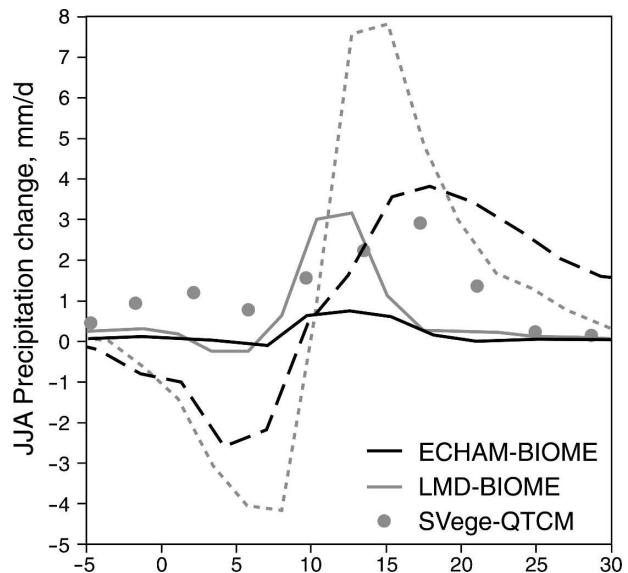


FIG. 8. JJA precipitation change (mm day^{-1}) over Africa (20°W – 30°E) for 6–0 kyr B.P. orbital conditions plotted from 5°S to 30°N . Two 20-yr GCM runs are coupled to the BIOME model: ECHAM (black lines) and LMD (gray lines) with dry (solid lines) and green (dashed lines) Sahara initial conditions. QTCM–SVEge results are the gray dots. Figure modified from de Noblet-Ducoudré et al. (2000).

sitivity is of similar magnitude to the GCMs. Note that findings from other work suggest that the presence of multiple equilibria depend on very strong vegetation feedbacks and tend to be wiped out by climate variability (Zeng et al. 2002).

The differences between the experiments in Fig. 8 [e.g., a sharper response from the Laboratoire de Météorologie Dynamique (LMD) at lower latitudes in both initial condition runs and less poleward extent than the European Community–Hamburg (ECHAM) run] are due to the atmosphere in these GCM coupled runs since both have the same vegetation model. The QTCM–SVEge model appears to be a reasonable prototype if we perform experiments on the atmospheric dynamics to see to what extent the mechanisms interact.

c. Evaluating roles of interactive vegetation and reduced ventilation

The precipitation sensitivity when moisture advection anomalies are reduced by a factor of 0.3 is shown in Fig. 9. The monsoon advances farther poleward in a zonal pattern relative to Fig. 6 (which includes interactive vegetation but with full-strength ventilation). Particularly notable is the advance of the 200 mm yr^{-1} contour.

A comparison of the influence of orbital changes,

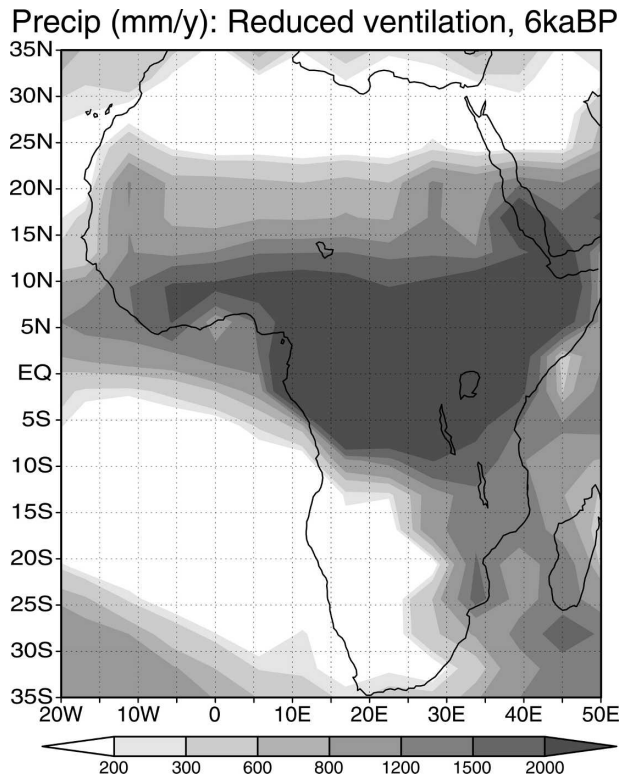


FIG. 9. Same as in Fig. 6, but with reduced anomalous ventilation.

interactive vegetation, and reduced ventilation is shown in Fig. 10. Figs. 10a,b show the differences between mid-Holocene and present-day orbital parameters with standard and reduced ventilation in the presence of interactive vegetation. Figs. 10c,d show the same differences without interactive vegetation. In this case, surface albedo is fixed to the 12-month climatology produced by the 0 kyr B.P. interactive vegetation experiment. Figure 10c is similar to a PMIP experiment but with an albedo consistent with our climatology. These are similar to the experiments of Su and Neelin (2005), without reducing the albedo (see section 1b).

A comparison of Figs. 10a and 10c shows that the interactive vegetation feeds back on the atmosphere enough to produce a stronger monsoon than in the fixed-albedo case in a latitude band approximately 12°–18°N. Interestingly, the poleward extent is not noticeably increased. When ventilation is reduced, the interactive vegetation plus reduced ventilation experiment (Fig. 10b) produces the most impact over a rather large expanse, in both monsoon intensity and poleward advance. This suggests that the interactive vegetation and the ventilation mechanism are interacting with each other for a combined effect. In the fixed-albedo case (Fig. 10d), the reduced ventilation appears to affect the

poleward extent even in the absence of vegetation feedbacks, while the latter contributes to enhance the magnitude of precipitation response. Similar to Stein and Alpert (1993), a measure of the synergy of the ventilation and vegetation effects can be estimated from the anomalies in Fig. 10 by considering the departures from Fig. 10c of Figs. 10a,d,b, respectively, as shown in Fig. 11. These measure the impact of interactive vegetation, ventilation, and the two acting together, relative to the effects of orbital parameters alone. The departures corresponding to both acting together are considerably larger in magnitude and spatial extent than the sum of the effects acting alone (Fig. 11). We note that the region of anomalies between approximately 20° and 25°N in Fig. 11b, corresponding to the shift of the poleward edge of the monsoon, is contributed to mainly by the change in ventilation.

The change in simulated LAI corresponding to Fig. 10 is shown in Fig. 12. For the fixed-albedo experiments, leaf area index is still calculated in the vegetation model from the soil moisture, but it is not permitted to feed back to the atmosphere through albedo or evapotranspiration. With interactive vegetation and reduced ventilation (Fig. 12b), the vegetation increases take the southern Sahara to a marginal grasslike state (with LAI around 0.5) as far north as about 22° or 23°N, a large increase over that produced by orbital factors and interactive vegetation alone (Fig. 12a). In the fixed-albedo orbital change experiment, the LAI increase is confined to the Sahel region with little poleward advance (shown in Fig. 12c). When reduced ventilation is added to the fixed-albedo experiment (Fig. 12d), there is some poleward advance of the monsoon, especially in the west. As seen in Fig. 3, SVEge is conservative in the LAI produced near the 200 mm yr⁻¹ precipitation line, so vegetation roughly corresponding to a dry grass vegetation type does not reach as far poleward as the 200 mm yr⁻¹ line in the precipitation change for this experiment (Fig. 10d). We note that the dominant impact of LAI changes is through the effect on albedo (Levis et al. 2004). For reference, the albedo averaged over 15°–30°N and 10°W–30°E from the last 20 yr of the 0 yr B.P. run is 37.6%. By definition, the fixed-albedo runs have the same albedo. In the 6 kyr B.P. interactive vegetation runs, albedo averaged over the same area from the last 20 yr of the run is 35.0%.

In a second set of experiments, we modify the ventilation in the control model as well as in the 6 kyr B.P. conditions. We do this in two ways: (i) reduce total ventilation by decreasing moisture advection and diffusion by one-half over Africa at each time step and (ii) modify only the moisture diffusion as a means of changing the ventilation. While these experiments do not iso-

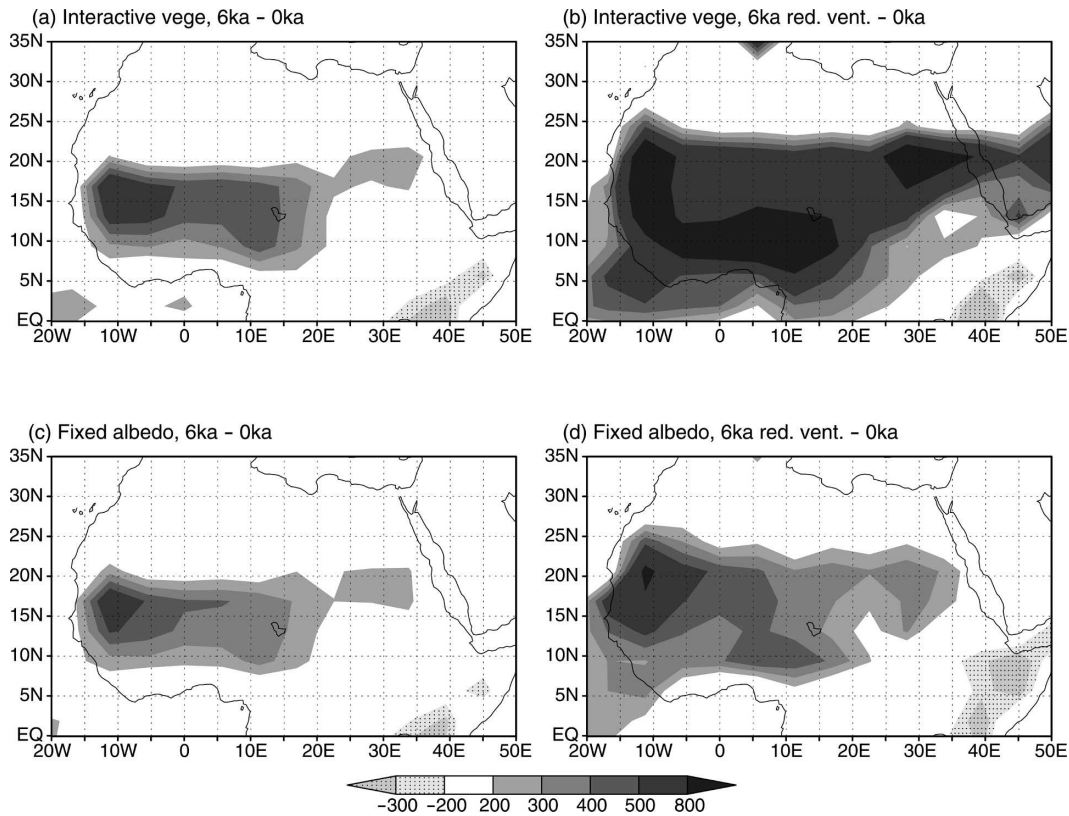


FIG. 10. Annual average precipitation change (mm yr^{-1}) for (a) 6–0 kyr B.P. interactive vegetation runs, (b) 6 kyr B.P. reduced anomalous ventilation minus 0 kyr B.P. interactive vegetation runs, (c) 6–0 kyr B.P. fixed-albedo runs, and (d) 6 kyr B.P. reduced anomalous ventilation minus 0 kyr B.P. fixed-albedo runs.

late the impact of ventilation on the 6 yr B.P. anomalies as neatly as those in Fig. 10, they provide complementary information. As discussed in section 4a, the climatology is not artificially controlled and thus these ex-

periments require new control 0 yr B.P. interactive vegetation runs.

The precipitation climatology from the reduced total ventilation (Fig. 13a) 0 kyr B.P. control run exhibits

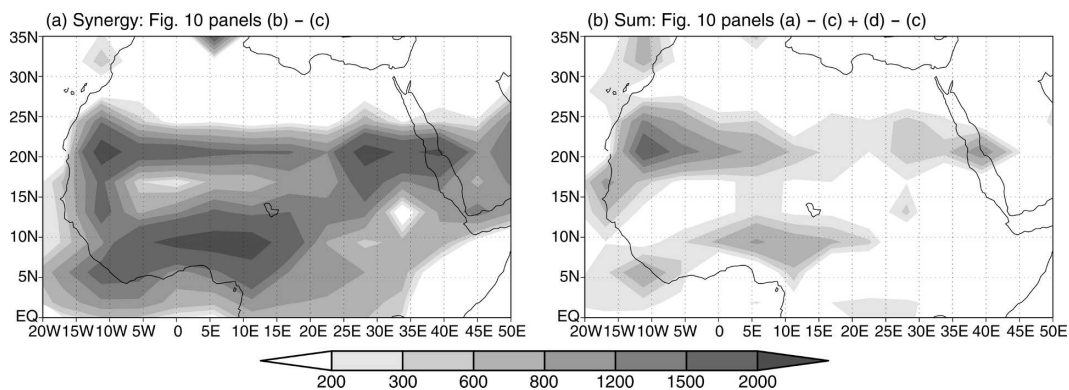


FIG. 11. An estimate of the synergy between changes in ventilation and interactive vegetation: differences between the annual average precipitation change (mm yr^{-1}) corresponding to the (a) synergy of interactive vegetation and reduced anomalous ventilation acting together (i.e., Fig. 10b minus Fig. 10c) and (b) sum of individual contributions of interactive vegetation and reduced anomalous ventilation (i.e., Fig. 10a - Fig. 10c + Fig. 10d - Fig. 10c).

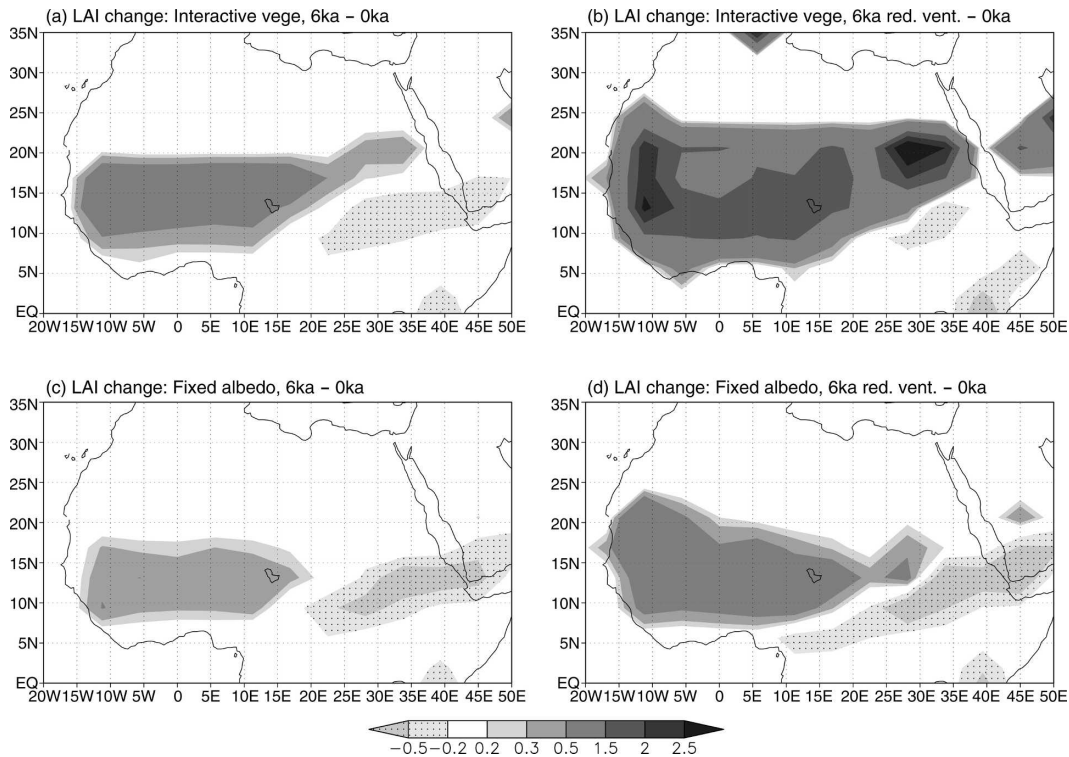


FIG. 12. Same as in Fig. 10, but for ASO LAI change. Note that in (c) and (d), LAI change is simply being used as a diagnostic of the impact of precipitation and evapotranspiration changes as they would affect vegetation and does not feed back in the model.

some differences from that of the standard control run (Fig. 2). In particular, the monsoon boundary extends slightly farther north in Fig. 13a, as expected since ventilation is reduced. The reduced diffusion control (Fig. 13c) is fairly close to the standard. By examining the 6 kyr B.P. changes relative to these respective controls, one can qualitatively compare the changes to the case with standard ventilation and interactive vegetation in Fig. 10a to see if the modified ventilation has had an impact. In doing so, the differences in climatology should be borne in mind.

Figure 13d shows that when only the diffusion is reduced, the monsoon change at 6 kyr B.P. is rather similar to that in the standard case, suggesting that the reduction in diffusion alone does not have that strong an impact. When the total ventilation is reduced (Fig. 13b), the monsoon changes are somewhat stronger and extend over a greater latitude range. The poleward boundary reaches about 23°N, as compared to about 19°N in the standard case (Fig. 10a), using the 200 mm yr^{-1} change contour as a measure. This is almost as far poleward as the reduced anomalous ventilation scenario in Fig. 10b (although a detailed comparison to this case is less relevant since the magnitude of the different reduced ventilation scenarios is not directly

comparable). We wish to emphasize the generally similar behavior of the monsoon under these two modifications to the model ventilation, reinforcing the conclusion that ventilation has a significant effect on the poleward extent of the mid-Holocene African monsoon.

d. Interactive vegetation and reduced ventilation effects on steppe boundary

To summarize key elements of our results, specifically for the steppe boundary, the northward reach of the 200 mm yr^{-1} annual precipitation contour is shown in Fig. 14. This view highlights the low precipitation areas, where the transition from desert to steppe conditions is estimated to occur in the Sahara with a precipitation increase of roughly 200–300 mm yr^{-1} (Jousaume et al. 1999). Using this precipitation measure allows a comparison to runs without interactive vegetation and sidesteps details of the vegetation model response at low precipitation. Maps for the 300 mm yr^{-1} annual precipitation contour look rather similar to Fig. 14, with a typical shift of one or two degrees of latitude toward the south.

As seen in Fig. 10, the most interesting case is when interactive vegetation and reduced ventilation act si-

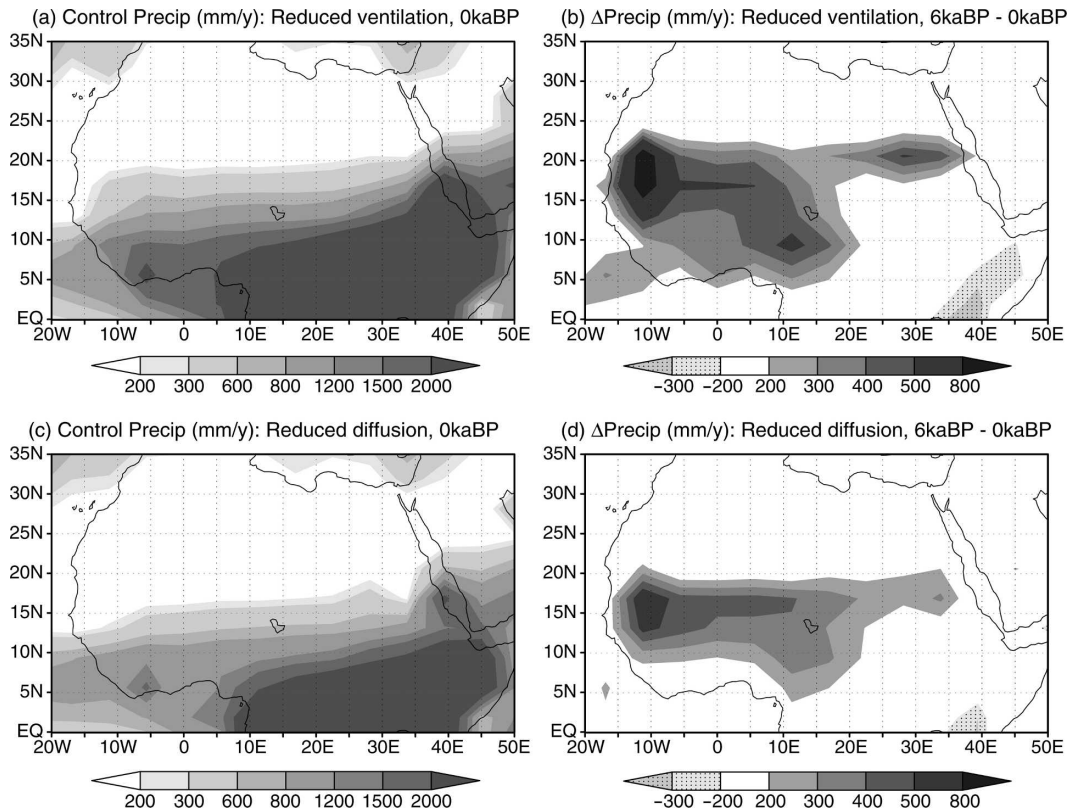


FIG. 13. Annual average precipitation (mm yr^{-1}) from the (a) 0 kyr B.P. reduced total ventilation control run, (b) change from 6–0 kyr B.P. reduced total ventilation run, (c) 0 yr B.P. reduced diffusion control run, and (d) change from 6–0 kyr B.P. reduced diffusion run. All experiments are with interactive vegetation.

multaneously. The other experiments offer a way of quantifying the sensitivity to each component. Two sets of experiments, interactive vegetation and fixed albedo, each of which have reduced ventilation experiments, are shown in Fig. 14. Although we show the two sets of experiments in two panels, we discuss each experiment in the order of enhanced effects.

As expected, the 0 kyr B.P. control run for the fixed-albedo case and the interactive vegetation case produces very similar results (Fig. 14). In the fixed-albedo case when mid-Holocene orbital parameters are implemented (Fig. 14a), the steppe boundary advances northward to approximately 20°N and becomes more zonal. In the interactive vegetation case with mid-

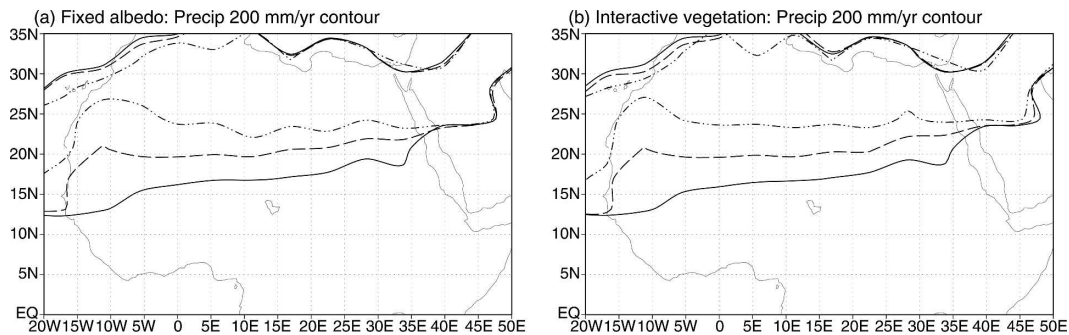


FIG. 14. The movement of the steppe boundary (200 mm yr^{-1} precipitation). The northward reach of the 200 mm yr^{-1} precipitation contour for two sets of experiments: the (a) fixed 0 yr B.P. SVege albedo and (b) interactive vegetation for 0 kyr B.P. (solid lines), 6 kyr B.P. (dashed lines), and 6 kyr B.P. reduced anomalous ventilation (dotted-dashed lines).

Holocene orbital parameters, the steppe boundary also reaches roughly 20°N, although as seen in Figs. 10a and 10c, there is an increase in monsoon intensity in the interactive case. When ventilation is reduced in the fixed-albedo case with mid-Holocene orbital parameters, the steppe boundary extends to about 24°N (averaged over 15°W–20°E), a change of about 4° relative to the orbital parameter-only case. The impact with the reduced ventilation shows the importance of the ventilation mechanism even in the absence of vegetation feedbacks. Clearly, the ventilation has a significant effect whether or not interactive vegetation is included. For the case with interactive vegetation, reduced ventilation, and mid-Holocene orbital parameters (Fig. 14b), the 200 mm yr⁻¹ precipitation contour also shifts to approximately 24°N (averaged 15°W–20°E). The steppe boundary thus seems to be strongly controlled by ventilation with or without interactive vegetation. The difference between the reduced ventilation case and the others in Fig. 14b can be interpreted as a rough measure of dynamic feedbacks in the presence of interactive vegetation.

5. Conclusions

The present study supports the importance of interactive vegetation, on the one hand, in changing the mid-Holocene North African monsoon (e.g., Claussen and Gayler 1997; Texier et al. 1997; Pollard et al. 1998; Claussen et al. 1999; Doherty et al. 2000; de Noblet-Ducoudré et al. 2000). On the other hand, the study also provides evidence of the importance of the ventilation mechanism in affecting the poleward boundary of the monsoon, especially in the absence of fixed high albedo that would prevent the monsoon from advancing poleward (Chou et al. 2001; Chou and Neelin 2003; Su and Neelin 2005). The impact of ventilation appears to help explain differences between GCMs running the same vegetation model (de Noblet-Ducoudré et al. 2000) and gives a mechanism by which differences in the atmospheric dynamics can influence the monsoon. This suggests that overly strong ventilation may be a factor in the poor simulation of mid-Holocene climate in some modeling studies. While estimating the strength of ventilation under paleo-conditions is difficult, awareness of the importance of this mechanism may be useful information to modelers evaluating their results. If a model is underresponsive in paleo-conditions, the model ventilation in current climate conditions can be compared to estimates of current observed ventilation seeking evidence for excessive strength in this factor. One key point indicated here is the importance of synergy between the ventilation

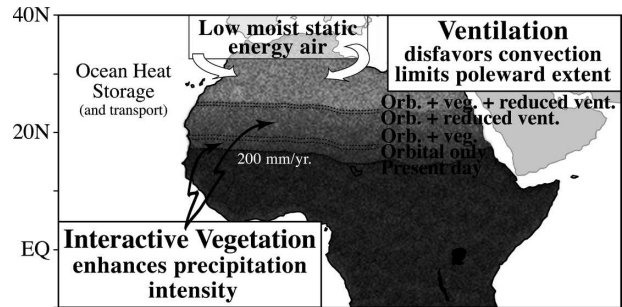


FIG. 15. Schematic diagram of ventilation and interactive vegetation mechanisms affecting the extent of the North African monsoon. Strong ventilation disfavors convection by bringing low moist static energy air over the continent from the oceans, and thus holds back the poleward advance of the monsoon. Interactive vegetation can act to reduce the high albedo values over the present-day Sahara Desert and can more effectively add moisture to the atmosphere, contributing to stronger monsoon intensity. The contour of present-day 200 mm yr⁻¹ annual average precipitation is shown as a measure of the monsoon boundary. Added to this is the poleward shift of the 200 mm yr⁻¹ line from various experiments (approximately the 20°W–20°E land area zonal average of the latitude shifts of the 200 mm yr⁻¹ contours in Fig. 14). These, respectively, represent the effects from 6 kyr B.P. orbital parameters with fixed albedo, interactive vegetation, fixed albedo and reduced ventilation, and interactive vegetation and reduced ventilation.

mechanism and interactive vegetation. Here we use two types of experiments to study this. One type artificially reduces ventilation, as it acts only on the *changes* (relative to the control) in moisture advection and diffusion so as to have an approximately similar control experiment to the model run without the change in dynamics. Other experiments alter the model total advection and/or diffusion (with 6 kyr B.P. changes being evaluated relative to the resulting 0 kyr B.P. control climatology, which differs from the standard control). Both ways of modifying the dynamics indicate that for substantial poleward movement of the monsoon boundary to occur for mid-Holocene parameters, the ventilation must not be overly strong. This holds with or without enhancement due to interactive vegetation. Furthermore, the impact of interactive vegetation and changes in ventilation acting together creates larger changes in precipitation than the sum of the effects individually (Fig. 11).

Another main point is that for a given magnitude of ventilation, interactive vegetation tends to enhance the monsoon in regions where orbital parameters give increased precipitation but is not very effective at moving the boundary of the monsoon poleward. Thus, although there is evidence that high albedo values over the Sahara prevent the poleward advance of the monsoon (Chou and Neelin 2003), interactive vegetation does not have much effect in moving the steppe boundary, as

measured by the 200 mm yr⁻¹ precipitation line. On the other hand, the strength of the ventilation has considerable effects on the poleward boundary of the monsoon and steppe boundary when orbital parameters are changed.

Our results are summarized in Fig. 15 where the shift of the 200 mm yr⁻¹ precipitation boundary is schematized consistent with experimental results. Changing the orbital parameters to 6 kyr B.P. moves the monsoon–steppe boundary poleward. Adding interactive vegetation does not move the boundary much farther, but enhances the precipitation and vegetation in regions that already receive some precipitation. Reduced ventilation shifts the boundary farther poleward. Combining interactive vegetation with the reduced ventilation does not shift the boundary farther but enhances precipitation behind it.

Acknowledgments. This research was supported by the National Science Foundation Grant ATM-0082529. The authors wish to thank J. Meyerson for graphical assistance and H. Su for discussion and the reduced ventilation code.

REFERENCES

- Barkstrom, B. R., E. F. Harrison, and R. B. Lee, 1990: Earth radiation budget experiment, preliminary seasonal results. *Eos, Trans. Amer. Geophys. Union*, **71**, 297–304.
- Bonfils, C., N. de Noblet-Ducoudré, P. Braconnot, and S. Joussaume, 2001: Hot desert albedo and climate change: Mid-Holocene monsoon in North Africa. *J. Climate*, **14**, 3724–3737.
- Braconnot, P., Ed., 2000: Paleoclimate Modeling Intercomparison Project (PMIP). WMO Tech. Doc. 1007, WCRP-111, 271 pp.
- , S. Joussaume, O. Marti, and N. de Noblet, 1999: Synergistic feedbacks from ocean and vegetation on the African monsoon response to mid-Holocene insolation. *Geophys. Res. Lett.*, **26**, 2481–2484.
- , O. Marti, S. Joussaume, and Y. Leclainche, 2000: Ocean feedback in response to 6 kyr B.P. insolation. *J. Climate*, **13**, 1537–1553.
- Chou, C., and J. D. Neelin, 2003: Mechanisms limiting the northward extent of the northern summer convection zones. *J. Climate*, **16**, 406–425.
- , —, and H. Su, 2001: Ocean–atmosphere–land feedbacks in an idealized monsoon. *Quart. J. Roy. Meteor. Soc.*, **127**, 1869–1891.
- Claussen, M., and V. Gayler, 1997: The greening of Sahara during the mid-Holocene: Results of an interactive atmosphere–biome model. *Global Ecol. Biogeogr. Lett.*, **6**, 369–377.
- , C. Kubatzki, V. Brovkin, and A. Ganopolski, 1999: Simulation of an abrupt change in Saharan vegetation in the mid-Holocene. *Geophys. Res. Lett.*, **26**, 2037–2040.
- DeFries, R. S., and J. R. G. Townshend, 1994: NDVI-derived land cover classifications at a global scale. *Int. J. Remote Sens.*, **15**, 3567–3586.
- DeMenocal, P. B., J. Ortiz, T. Guilderson, J. Adkins, M. Sarnthein, L. Baker, and M. Yarusinsky, 2000: Abrupt onset and termination of the African humid period: Rapid climate responses to gradual insolation forcing. *Quat. Sci. Rev.*, **19**, 347–361.
- de Noblet-Ducoudré, N., M. Claussen, and C. Prentice, 2000: Mid-Holocene greening of the Sahara: First results of the GAIM 6000 yr B.P. experiment with two asynchronously coupled atmosphere/biome models. *Climate Dyn.*, **16**, 643–659.
- Dickinson, R. E., A. Henderson-Sellers, and P. J. Kennedy, 1993: Biosphere–Atmosphere Transfer Scheme (BATS) version 1e as coupled to the NCAR Community Climate Model. NCAR Tech. Note NCAR/TN-387+STR, Boulder, CO, 72 pp.
- Doherty, R., J. Kutzbach, J. Foley, and D. Pollard, 2000: Fully-coupled climate/dynamical vegetation model simulations over Northern Africa during the mid-Holocene. *Climate Dyn.*, **16**, 561–573.
- Dupont, L. M., 1993: Vegetation zones in NW Africa during the Brunhes chron reconstructed from marine palynological data. *Quat. Sci. Rev.*, **12**, 189–202.
- Entekhabi, D., and P. S. Eagleson, 1989: Land surface hydrology parameterization for atmospheric general circulation models including subgrid scale spatial variability. *J. Climate*, **2**, 816–832.
- Ganopolski, A., C. Kubatzki, M. Claussen, V. Brovkin, and V. Petoukhov, 1998a: The influence of vegetation–atmosphere–ocean interaction on climate during the mid-Holocene. *Science*, **280**, 1916–1919.
- , S. Rahmstorf, V. Petoukhov, and M. Claussen, 1998b: Simulation of modern and glacial climates with a coupled global model of intermediate complexity. *Nature*, **391**, 351–356.
- Hales, K., J. D. Neelin, and N. Zeng, 2004: Sensitivity of tropical land climate to leaf area index: Role of surface conductance versus albedo. *J. Climate*, **17**, 1459–1473.
- Henderson-Sellers, A., Z.-L. Yang, and R. E. Dickinson, 1993: The Project for Intercomparison of Land-surface Parameterization Schemes. *Bull. Amer. Meteor. Soc.*, **74**, 1335–1349.
- Hewitt, C. D., and J. F. B. Mitchell, 1998: A fully coupled GCM simulation of the climate of the mid-Holocene. *Geophys. Res. Lett.*, **25**, 361–364.
- Irizarry-Ortiz, M. M., G. L. Wang, and E. A. B. Eltahir, 2003: Role of the biosphere in the mid-Holocene climate of West Africa. *J. Geophys. Res.*, **108**, 4042, doi:10.1029/2001JD000989.
- Jolly, D., S. P. Harrison, B. Damnati, and R. Bonnefille, 1998a: Simulated climate and biomes of Africa during the Late Quaternary: Comparison with pollen, and lake status data. *Quat. Sci. Rev.*, **17**, 629–658.
- , and Coauthors, 1998b: Biome reconstruction from pollen and plant macrofossil data for Africa and the Arabian peninsula at 0 and 6 ka. *J. Biogeogr.*, **25**, 1007–1027.
- Joussaume, S., and K. E. Taylor, 1995: Status of the Paleoclimate Modeling Intercomparison Project (PMIP). *Proc. First Int. AMIP Scientific Conf.*, WCRP Rep. 92, WMO Tech. Doc. 732, Monterey, CA, AMIP, 425–430.
- , and Coauthors, 1999: Monsoon changes for 6000 years ago: Results of 18 simulations from the Paleoclimate Modeling Intercomparison Project (PMIP). *Geophys. Res. Lett.*, **26**, 859–862.
- Koster, R. D., and P. C. D. Milly, 1997: The interplay between transpiration and runoff formulations in land surface schemes used with atmospheric models. *J. Climate*, **10**, 1578–1591.
- Kutzbach, J. E., and Z. Liu, 1997: Response of the African mon-

- soon to orbital forcing and ocean feedbacks in the Middle Holocene. *Science*, **278**, 440–443.
- , P. J. Bartlein, J. A. Foley, S. P. Harrison, S. W. Hostetler, Z. Liu, I. C. Prentice, and T. Webb III, 1996a: Potential role of vegetation feedback in the climate sensitivity of high-latitude regions: A case study at 6000 years B.P. *Global Biogeochem. Cycles*, **10**, 727–736.
- , G. Bonan, J. Foley, and S. Harrison, 1996b: Vegetation and soil feedbacks on the response of the African monsoon to forcing in the early to middle Holocene. *Nature*, **384**, 623–626.
- Levis, S., G. B. Bonan, and C. Bonfils, 2004: Soil feedback drives the mid-Holocene North African monsoon northward in fully coupled CCSM2 simulations with a dynamic vegetation model. *Climate Dyn.*, **23**, 791–802.
- Los, S. O., and Coauthors, 2000: A global 9-yr biophysical land surface dataset from NOAA AVHRR data. *J. Hydrometeorol.*, **1**, 183–199.
- Neelin, J. D., and N. Zeng, 2000: A quasi-equilibrium tropical circulation model—Formulation. *J. Atmos. Sci.*, **57**, 1741–1766.
- Petit-Maire, N., 1989: Interglacial environments in presently hyperarid Sahara: Paleoclimatic implications. *Paleoclimatology and Paleometeorology: Modern and Past Patterns of Global Atmospheric Transport*, M. Leinen and M. Sarnthein, Eds., Kluwer Academic, 637–661.
- Pollard, D., J. C. Bergengren, L. M. Stillwell-Soller, B. Felzer, and S. L. Thompson, 1998: Climate simulations for 10 000 and 6000 years B.P. using the GENESIS global climate model. *Paleoclim. Data Modell.*, **2**, 183–218.
- Prentice, I. C., and T. Webb III, 1998: BIOME 6000: Reconstructing global mid-Holocene vegetation patterns from palaeoecological records. *J. Biogeogr.*, **25**, 997–1005.
- , W. Cramer, S. P. Harrison, R. Leemans, R. A. Monserud, and A. M. Solomon, 1992: A global biome model based on plant physiology and dominance, soil properties, and climate. *J. Biogeogr.*, **19**, 117–134.
- , D. Jolly, and BIOME-6000-Participants, 1998: Mid-Holocene and glacial-maximum vegetation geography of the northern continents and Africa. *J. Biogeogr.*, **25**, 997–1005.
- Ruddiman, W. F., and A. C. Mix, 1993: The north and equatorial Atlantic at 9000 and 6000 yr B.P. *Global Climates since the Last Glacial Maximum*, H. E. Wright Jr. et al., Eds., University of Minnesota Press, 94–135.
- Sarnthein, M., 1978: Sand deserts during glacial maximum and climatic optimum. *Nature*, **272**, 43–46.
- Sellers, P. J., S. O. Los, C. J. Tucker, C. O. Justice, D. A. Dazlich, G. J. Collatz, and D. A. Randall, 1994: A global 1 by 1 degree NDVI data set for climate studies. Part 2: The generation of global fields of terrestrial biophysical parameters from the NDVI. *Int. J. Remote Sens.*, **15**, 3519–3545.
- , and Coauthors, 1996a: A revised land surface parameterization (SiB2) for atmospheric GCMs. Part I: Model formulation. *J. Climate*, **9**, 676–705.
- , S. O. Los, C. J. Tucker, C. O. Justice, D. A. Dazlich, G. J. Collatz, and D. A. Randall, 1996b: A revised land surface parameterization (SiB2) for atmospheric GCMs. Part II: The generation of global fields of terrestrial biophysical parameters from satellite data. *J. Climate*, **9**, 706–737.
- Shuttleworth, W. J., 1988: Evaporation from Amazonian rain forest. *Proc. Roy. Soc. London*, **B233**, 321–346.
- Stein, U., and P. Alpert, 1993: Factor separation in numerical simulations. *J. Atmos. Sci.*, **50**, 2107–2115.
- Street, F. A., and A. T. Grove, 1976: Environmental and climatic implications of late Quaternary lake-level fluctuations in Africa. *Nature*, **261**, 385–390.
- Street-Perrott, F. A., and S. P. Harrison, 1985: Lake levels and climate reconstructions. *Paleoclimate Analysis and Modeling*, A. D. Hecht, Ed., John Wiley and Sons, 291–340.
- , and R. A. Perrott, 1993: Holocene vegetation, lake levels and climate of Africa. *Global Climates since the Last Glacial Maximum*, H. E. Wright Jr. et al., Eds., University of Minnesota Press, 318–356.
- , J. F. B. Mitchell, D. S. Marchand, and J. S. Brunner, 1990: Milankovitch and albedo forcing of the tropical monsoon: A comparison of geological evidence and numerical simulations for 9000 y B.P.. *Trans. Roy. Soc. Edinburgh: Earth Sci.*, **81**, 407–427.
- Su, H., and J. D. Neelin, 2005: Dynamical mechanisms for African monsoon changes during the mid-Holocene. *J. Geophys. Res.*, **110**, D19105, doi:10.1029/2005JD005806.
- Texier, D., and Coauthors, 1997: Quantifying the role of biosphere–atmosphere feedbacks in climate change: Coupled model simulations for 6000 years B.P. and comparison with paleodata for northern Eurasia and northern Africa. *Climate Dyn.*, **13**, 865–882.
- Wright, I. R., and Coauthors, 1996: Towards a GCM surface parameterization of Amazonia. *Amazonian Deforestation and Climate*, J. H. C. Gash et al., Eds., John Wiley and Sons, 473–504.
- Xie, P., and P. A. Arkin, 1997: Global precipitation: A 17-year monthly analysis based on gauge observations, satellite estimates, and numerical model outputs. *Bull. Amer. Meteor. Soc.*, **78**, 2539–2558.
- Xue, Y., 1991: A two-dimensional coupled biosphere–atmosphere model and its application. *Adv. Atmos. Sci.*, **8**, 447–458.
- Yu, G., and S. Harrison, 1996: An evaluation of the simulated water balance of Eurasia and northern Africa at 6000 yr B.P. using lake status data. *Climate Dyn.*, **12**, 723–735.
- Zeng, N., and J. D. Neelin, 1999: A land–atmosphere interaction theory for the tropical deforestation problem. *J. Climate*, **12**, 857–872.
- , and —, 2000: The role of vegetation–climate interaction and interannual variability in shaping the African Savanna. *J. Climate*, **13**, 2665–2670.
- , —, K.-M. Lau, and C. J. Tucker, 1999: Enhancement of interdecadal climate variability in the Sahel by vegetation interaction. *Science*, **286**, 1537–1540.
- , —, and C. Chou, 2000: A quasi-equilibrium tropical circulation model-implementation and simulation. *J. Atmos. Sci.*, **57**, 1767–1796.
- , K. Hales, and J. D. Neelin, 2002: Nonlinear dynamics in a coupled vegetation–atmosphere system and implications for desert–forest gradient. *J. Climate*, **15**, 3474–3487.